Vol. 437: 147–164, 2011
doi: 10.3354/meps09268

MARINE ECOLOGY PROGRESS SERIES
Mar Ecol Prog Ser

Published September 15

OPEN ACCESS

The exhalant jet of mussels *Mytilus edulis*

Hans Ulrik Riisgård[1,*], Bo Hoffmann Jørgensen[2], Kim Lundgreen[1], Francesca Storti[2], Jens Honore Walther[2,3], Knud Erik Meyer[2], Poul S. Larsen[2]

[1]Marine Biological Research Centre, University of Southern Denmark, Hindsholmvej 11, 5300 Kerteminde, Denmark
[2]DTU Mechanical Engineering, Fluid Mechanics, Technical University of Denmark, Building 403, 2800 Kgs. Lyngby, Denmark
[3]Chair of Computational Science, ETH Zurich, 8092 Switzerland

ABSTRACT: The exhalant jet flow of mussels in conjunction with currents and/or other mussels may strongly influence the mussels' grazing impact. Literature values of mussel exhalant jet velocity vary considerably and the detailed fluid mechanics of the near-mussel flow generated by the exhalant jet has hitherto been uncertain. Computational modelling of this phenomenon depends on knowledge of the velocity distribution near the exhalant siphon aperture of mussels to provide appropriate boundary conditions for numerical flow models. To be useful such information should be available for a range of mussel shell lengths. Here, we present results of a detailed study of fully open mussels *Mytilus edulis* in terms of filtration rate, exhalant siphon aperture area, jet velocity, gill area and body dry weight, all as a function of shell length (mean ± SD) over the range 16.0 ± 0.4 to 82.6 ± 2.9 mm, with the corresponding scaling laws also presented. The exhalant jet velocity was determined by 3 methods: (1) measured clearance rate divided by exhalant aperture area, (2) manual particle tracking velocimetry (PTV) using video-microscope recordings, and (3) particle image velocimetry (PIV). The latter provides detailed 2-component velocity distributions near the exhalant siphon in 5 planes parallel to the axis of the jet and the major axis of the oval aperture, and hence estimates of momentum and kinetic energy flows in addition to mean velocity. Data obtained on particles inside the exhalant jet of filtered water was verified by the use of titanium dioxide seeding particles which were de-agglomerated by ultrasound to a size range of 0.7 to 2 µm prior to addition, to avoid retention by the gill filter of the mussels. We found that exhalant jet velocity was essentially constant at ~8 cm s^{-1}, and independent of shell length. Based on geometric similarity and scaling of mussel pump-system characteristics we found that these characteristics coincide approximately for all sizes when expressed as pressure head versus volume flow divided by shell length squared.

KEY WORDS: Filtration rate · Exhalant siphon area · Particle image velocimetry · Particle tracking velocimetry · Exhalant jet velocity · Velocity field · Allometric equation · Scaling law

INTRODUCTION

Filter-feeding bivalves process large amounts of ambient water to acquire the food needed for sustaining life, and extensive literature deals with the amounts of water pumped through the gills of a mussel and the efficiency by which suspended particles are retained (Møhlenberg & Riisgård 1978, 1979, Jørgensen 1990, Riisgård 2001a, Riisgård & Larsen 2010). Nevertheless, there is considerable variation between published values of the exhalant jet velocity of mussels (Jørgensen et al. 1986, 1988, André et al. 1993, Newell et al. 2001, Stamhuis 2006, Maire et al. 2007, Frank et al. 2008, MacDonald et al. 2009, Troost et al. 2009), and little is known about the detailed fluid mechanics of flow near a mussel that is generated by the flow through the exhalant siphon appearing as a well structured jet (André et al. 1993, Green et al. 2003). This flow in conjunction with a possible imposed external flow from currents or other mussels

*Email: hur@biology.sdu.dk

will influence the grazing impact and thus the concentration distribution of food particles reaching the inhalant aperture; hence affecting the feeding conditions of the mussel. Of particular interest is the undesirable phenomenon of re-filtration where part of the once filtered and exhaled water reaches the inhalant aperture of either the same or other mussels. This has been studied to some extent for mussel beds where a number of attempts have been made to model phytoplankton concentration gradients caused by dense beds of filter-feeding bivalves in relatively strong currents with a high degree of turbulence (Wildish & Kristmanson 1984, 1997, Fréchette & Bourget 1985, Fréchette et al. 1989, O'Riordan et al. 1993, Butman et al. 1994, Mann & Lazier 1996, Herman et al. 1999, Jonsson et al. 2005, Tweddle et al. 2005, Lassen et al. 2006). Moderate currents may generate enough turbulence in the benthic boundary layer to increase the supply of food to the filter feeders by turbulent mixing. However, the additional 'biomixing' induced by the filter feeders themselves (Larsen & Riisgård 1997) has not yet been included in any model. Similar considerations may also be important for dense populations of mussels in nature (Riisgård et al. 2004, 2007) and in aquaculture systems (Newell et al. 1998, Angel et al. 2002, Petersen et al. 2008, Maar et al. 2008, Plew et al. 2009, Duarte et al. 2010). Further progress in understanding and optimizing such systems relies on computational modelling and supporting experiments.

It is therefore of interest to describe the exhalant jet of *Mytilus edulis* in terms of its oval shape at the siphon aperture, its velocity, spreading rate, penetration, and breakup. One aspect of this issue is the velocity distribution near the exhalant aperture, which is needed to provide appropriate boundary conditions for numerical flow models and to estimate the actual flows of momentum and kinetic energy that are important for biomixing and mussel pump modelling. To be useful such results should be available for a range of typical mussel sizes, for example in terms of shell length. Several experimental techniques exist for measuring velocities: Particle Image Velocimetry (PIV), Particle Tracking Velocimetry (PTV), Laser Doppler Anemometry (LDA) and hot-film anemometry or thermistor probes (for a mini-review of techniques used for analysing flow in zoobenthos see Riisgård & Larsen 2005). In the present study we have chosen 2-component PIV to investigate the exhalant flow of *M. edulis* because of the ability of the method to map a 2-dimensional field of velocities simultaneously, thereby providing insight into complicated flow structures in a convenient way. Secondly, we have used PTV based on manual tracking of entrained particles by microscope video recordings to further characterize the exhalant jet. As a third approach, mean exhalant jet velocities were calculated from measured clearance rates divided by aperture area.

MATERIALS AND METHODS

Experimental mussels

Blue mussels *Mytilus edulis* were collected in Kerteminde Fjord, Denmark, and acclimated in the laboratory at the Marine Biological Research Centre, University of Southern Denmark, for 1 wk prior to the experiments. The mussels were kept in aerated flow-through tanks supplied with seawater from the fjord inlet. During the experimental period water temperature and salinity were 11.6 ± 0.2°C and 19.8 ± 1.2 psu (means ± SD), respectively.

Filtration rate

Filtration rates were measured as the volume of water cleared of suspended particles per unit of time. The reduction in the number of particles as a function of time was followed by taking water samples (10 ml) at fixed time intervals from an aquarium containing mussels in well-mixed seawater, to which algal cells *Rhodomonas salina* were added, and measuring the particle concentration with an electronic particle counter (Elzone 5380). The algal cells had a diameter of ~6 µm and were therefore retained by the gills of the mussels with 100% efficiency (Møhlenberg & Riisgård 1978). The filtration rate (F) was determined from the exponential decrease in algal concentration as a function of time using the usual clearance formula (e.g. Coughlan 1969, Jørgensen 1990):

$$F = (V/t \times n) \ln(C_0/C_t) = V/n \times b \quad (1)$$

where C_0 and C_t are initial and terminal concentrations of particles, V = water volume in aquarium, t = time, n = number of mussels and b is the slope of the regression line in a semi-ln plot for the reduction in algal concentration with time in a well-mixed aquarium, hence:

$$F = V \times b/n \quad (2)$$

A control experiment without mussels showed that sedimentation of algal cells was insignificant. In all experiments, the algal concentration was kept below

4000 *Rhodomonas* cells ml^{-1} (equivalent to 5 µg chl *a* l^{-1}, Clausen & Riisgård 1996) which is below the threshold concentration for pseudofaeces production and incipient saturation reduction of filtration activity (Riisgård 2001b).

Exhalant siphon area and shell opening degree

Exhalant siphon cross-sectional area (*ESA*) was measured by 2 methods (M1, M2). M1: a ruler was placed in the transparent experimental plastic aquarium close to the mussel and, from digital photos, the maximal (2*a*) and minimal (2*b*) widths of the oval exhalant opening (Fig. 1C) were measured manually with a ruler. The *ESA* was subsequently calculated using the formula for an ellipse: $ESA = \pi ab$. M2: the exhalant cross-sectional area was cut from an enlarged paper photo and *ESA* was determined by multiplying the weight of the cut of paper with a measured conversion factor (i.e. weight of one area unit of paper). Mussel shell opening degree (*SOD*) was defined as the distance between the shells just below the exhalant siphon aperture (Fig. 1C), and it was measured manually from a digital photo by using a ruler placed in the experimental tank next to the mussel.

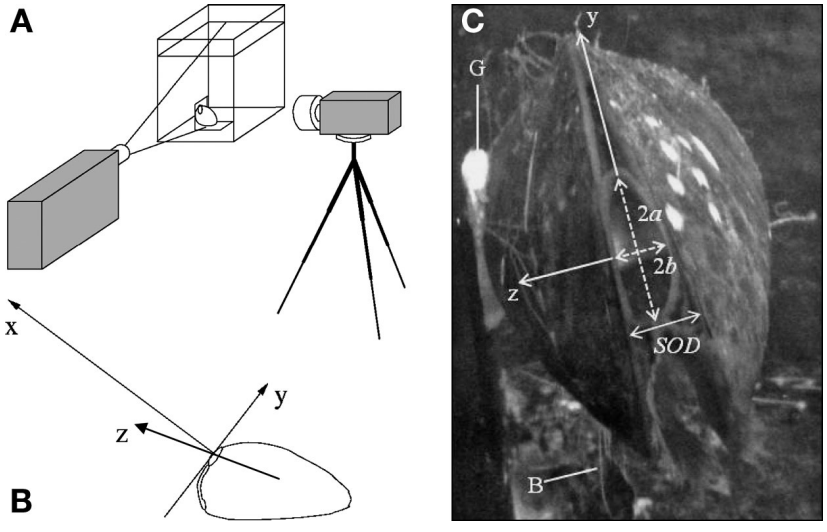

Fig. 1. *Mytilus edulis*. (**A**) Experimental setup used for particle image velocimetry (PIV), consisting of a water filled transparent plastic aquarium with the mussel positioned at the bottom, a laser sheet for illuminating the fluid in a plane aligned with the axis of the jet, and a digital camera. (**B**) Coordinate system at aperture of mussel: center line of the jet is *x*-axis, laser sheet is positioned in 5 *x*,*y*-planes spaced 1.0 mm apart from $z = -2$ to $+2$ mm. (**C**) Photo of mussel showing maximal (2*a*) and minimal (2*b*) widths of the oval exhalant aperture and shell opening degree (*SOD*); B = byssus threads; G = glue for fixing mussel to bracket post

Gill area, body dry weight, and condition index

To measure the gill area, mussels were cut open and seawater was added to one of the shells to allow the gill to unfold so that its outline could be drawn on a piece of transparent film (Arkwright). The area of a single gill layer (i.e. 1 lamella) was measured from the weight of the drawing on the transparent film, and this value was subsequently multiplied by 8 (2 W-shaped gills, each with 2 demibranchs with 2 lamellae of same size, e.g. Jørgensen 1990, his Fig. 2) to obtain the total gill area (*G*) of the mussel.

Dry weight of the soft body (*W*, mg) was measured after drying it in an oven at 90°C for 24 h. The condition index (*CI*) of the mussels was calculated as:

$$CI = W/L^3 \quad (3)$$

where *L* is the shell length (cm).

Exhalant jet velocity from clearance rate and particle tracking velocimetry

The mean velocity of the exhalant jet (V_e) was calculated as:

$$V_e = F/ESA \quad (4)$$

In addition, paths of naturally occurring particles (<40 µm) near to the exhalant siphon region of a 30 mm shell length actively feeding mussel *Mytilus edulis*, fed algal cells *Rhodomonas salina*, were recorded using a video camera and a 50 half-frames-per-second video recorder (Panasonic NV-FS200 HQ) attached to a horizontal dissecting microscope (Wild M3C) placed in front of an observation chamber holding the mussel. Video frames could be copied to paper by means of a video graphic printer (Sony UP-860 CE), and the relative movements of particles were traced from their position in successive frames, with time intervals of 0.1 or 0.02 s. The main purpose of the video recordings was to trace the path and measure the speed of particles close to the exhalant siphon opening as a different method of obtaining exhalant jet velocities.

Experimental setup for particle image velocimetry

Particle Image Velocimetry (PIV) was utilized for measuring the velocity field in the area of the exhalant jet from a mussel in still water as shown in the schematic setup in Fig. 1A. The PIV method has been described in detail by e.g. Raffel et al. (2007), and used in studies of bivalves by Stamhuis (2006), Frank et al. (2008), and Troost et al. (2009). A camera takes 2 consecutive images of the particles moving with the fluid in the plane illuminated by a laser sheet. The displacement between the images determines the velocity given the time interval between the frames. The double cavity YAG laser (New Wave Research Solo 120XT-15 Hz) emits 2 short (5 ns) pulses every 250 ms. The emitted energy in each pulse is 24 to 60 mJ. Frequency doubling transforms the light to the wave length 532 nm. The laser optics generates a laser sheet with a beam waist of 2 mm, which is further reduced to 0.5 mm by a lens with a focal length of 237 mm. The laser was mounted on a traversing bench allowing positioning of the laser sheet relative to the mussel which was fixed to a bracket post with 2-component styrene monomer glue (Plastic Padding, 'Chemical Metal') to avoid movement. Prior to the experiment, metal sheets placed at the rear, back, and bottom surfaces of the tank were painted black in order to avoid reflections of laser light. A Dantec HiSense PIV/PLIF camera was mounted on a tripod resting on the floor. The camera has a focal length of 62 mm and a CCD chip with resolution 1280 × 1024 measuring 8.75 × 7.00 mm. The camera was connected to a camera controller (Dantec HiSense) and synchronized with the laser using a timer box (Dantec); all connected to a computer utilizing the Dantec software DynamicStudio ver. 3.00. In order to operate the camera in daylight, it was fitted with a green filter that only transmitted scattered laser light.

A small particle size is needed to resolve the exhalant flow because 50% of the particles with diameter 1.0 µm are retained by the mussels and nearly all the particles are retained for diameters >2.0 µm (Møhlenberg & Riisgård 1978). Titanium dioxide (TiO_2) particles, previously used by Frank et al. (2008), were used as seeding in the following way. A small amount of TiO_2 powder was suspended in ethanol and diluted with water. To break up agglomerated particles, an ultrasound device (Struers Metason 200 HT) was used. The suspension of particles was kept in a glass bottle and treated with ultrasound in a water bath for 60 min. A sample of the resulting contents of the bottle was examined under a microscope which showed the typical particle size to be within the range of 0.7 to 2 µm. A sufficient amount of suspended particles were added to the observation aquarium to ensure a particle concentration of 10 µg l^{-1}. An aperture of *f*-number = 4.0 was chosen for the camera. The TiO_2 particles turned out to be sufficiently bright, despite their small size. Further, clearance rate experiments with *Rhodomonas salina* and with and without TiO_2 particles added to a 5 l aquarium containing 5 mussels (mean ± SD shell length = 32.20 ± 0.94 mm) were conducted to evaluate if the TiO_2 particles affected the filtration rate. Neither 0.1 nor 0.2 mg TiO_2 l^{-1} (i.e. 10 and 20 times the concentrations used in the PIV experiments) had any influence on the filtration rate, which was measured to be 30.4 ± 1.8 ml min^{-1} $ind.^{-1}$. During PIV experiments, the mussels were fed *R. salina* algal cells. After each new addition of algal cells (up to 4000 cells ml^{-1}) the concentration in the observation aquarium, which was kept strongly mixed in the relatively short periods between PIV measurements (performed in stagnant water), was followed by taking samples (10 ml) at 5 to 10 min intervals using an electronic particle counter (Elzone 5380). Thus clearance rates (F) could be calculated and used along with estimates of *ESA* determined from digital photos of the exhalant opening to estimate the exhalant jet velocity (V_e), which was subsequently compared with the PIV measurements.

Because of the high Stokesian drag due to their small size and despite their high density (ρ_p = 4.26 g cm^{-3}) the TiO_2 particles closely follow the water flow to give correct measured velocities. However, during periods of no flow some settling of particles was observed. The terminal settling velocity is calculated as:

$$V_p = (g d_p^2/18\nu)\ (\rho_p/\rho - 1) \quad (5)$$

where g denotes the acceleration of gravity, and ν and ρ the kinematic viscosity and density of seawater, respectively. For diameters in the range d_p = 0.7 to 2 µm for particles assumed to be spherical, V_p = 0.9 to 7.1 µm s^{-1}. Furthermore, the ability of particles to follow changes in velocity is given by the characteristic time constant:

$$\tau_p = (\rho_p/\rho)\ (d_p^2/18\nu) \quad (6)$$

which takes the corresponding small values of τ_p = 0.95 to 0.12 µs.

Measurement procedure for particle image velocimetry

Prior to the velocity measurements, the length scale of the camera image was calibrated with a ruler placed near the mussel. For this, the green filter was

temporarily removed from the camera and then the laser sheet was adjusted to intersect the exhalant siphon and aligned with the jet axis (x) and the major axis (y) of the oval aperture. To do this, milk diluted with sea water was fed through the inhalant orifice to visualize the exhalant jet and the camera was focused on the laser sheet. Batches of typically 100 image pairs were used for analysis. Batches were taken at various locations across the oval aperture, with a spacing of 1 mm along the minor axis (z) (Fig. 1B). For each z-position, the filtration rate (F) of the mussel in question was determined by measuring the exponential decrease in concentration of algal cells in the observation aquarium at 5 to 10 min intervals and using Eq.(2).

Data processing for particle image velocimetry

To obtain velocity from the displacement of particles recorded in image pairs, the adaptive correlation with 50% overlap for an interrogation area of 32 × 32 pixels, available in the Dynamic Studio software, was used, yielding a resolution of 79 × 63 velocity vectors. The adaptive correlation is a variation of what is known as multiple pass interrogation with hierarchical grid refinement (Raffel et al. 2007). Velocity vectors were then validated by the moving average method. Care was taken to ensure that the maximum movement of the particles was <30% of the size of the interrogation area by limiting the time interval between the consecutive frames. After the screening, the vector average field as well as root mean square (rms) fields were calculated from the set of typically 100 vector fields. In the subsequent analysis, the data are referred to by the coordinate system shown in Fig. 1B. Here, the center line of the jet from the exhalant aperture of the mussel is oriented along the x-axis and the laser sheet is positioned in either of 5 x,y-planes spaced 1.0 mm apart from $z = -2$ to $+2$ mm along the minor axis of the oval aperture. Based on observed SDs in the range of 0.1 to 0.2 cm s^{-1}, the estimated uncertainty is ~2% on mean velocity vectors and ~15% on rms-velocities.

RESULTS

Estimated velocity of the exhalant jet from filtration rate and particle tracking velocimetry

Addition of algal cells to the aquaria with initially unfed groups of *Mytilus edulis* stimulated the mussels to fully open their valves within ~10 to 60 min, and this response was also reflected in increased filtration rates (F) (and thus steeper slopes of the linear regression lines) in the clearance experiments (Fig. 2, Table 1). Thus, data for the 5 groups of fully open and maximum filtering mussels (Table 2) could be separated from not fully open mussels with reduced filtration rate (Table 3). From Table 2 it appears that the estimated velocity (means ± SD) of the exhalant jet (V_e) in maximum filtering mussels was 8.3 ± 1.7 cm s^{-1} when Method 1 for estimating exhalant siphon area (*ESA*) was used and 6.4 ± 1.9 cm s^{-1} when Method 2 was employed. It is notable that the V_e seems to be independent of mussel shell length (Fig. 3). From Table 3 it appears that simultaneously measured F and *ESA* at 60 to 80% reduced *SOD* result in lower V_e (4.3 ± 1.0 cm s^{-1}) compared to that of fully open mussels (8.3 ± 1.7 cm s^{-1}) (Table 1).

The flow patterns and speeds obtained by PTV in the zone between inhalant and exhalant water of a 35 mm shell length mussel (20°C) are shown in Fig. 4. The exhalant jet is invisible because all particles in the inhalant water have been restrained by the gills, but particles in the ambient water close to the jet were accelerated, indicating an V_e of about 8.7 cm s^{-1} at a distance of ~15 mm above the exhalant aperture, which is in good agreement with the estimated velocity (Table 2, Method 1). Similar flow patterns for entrained particles are seen for a 56 mm shell length mussel (12°C) in Fig. 5 where the highest observed speeds were somewhat lower. Fig. 6 shows the fluorescein-visualized exhalant jets from a mussel. When the dye was sucked in through the inhalant opening as a very thin current from the dosing-pipette tip, only a thin ray of the jet was visualized, and this indicates that the flow is laminar through the mussel-gill filter pump (i.e. no mixing and dispersion takes place inside the mussel). The spreading of the jet is clearly visible (Fig. 6A) with a spreading half-angle of about 9.5°.

The filtration rate as a function of shell length (L), gill area (G) and body dry weight (W) are shown in Fig. 7, Fig. 8, and Fig. 9, respectively. Further, the *ESA*, *SOD* and W, all as a function of L, are shown in Fig. 10, Fig. 11 and Fig. 12, respectively. Finally, F as a function of *SOD* and *ESA* are shown in Fig. 13 and Fig. 14, respectively.

Velocity fields from particle image velocimetry

Data from 1 (logbook number 503) of 4 successful PIV experiments for mussels of decreasing shell length are shown in Table 4 along with the concen-

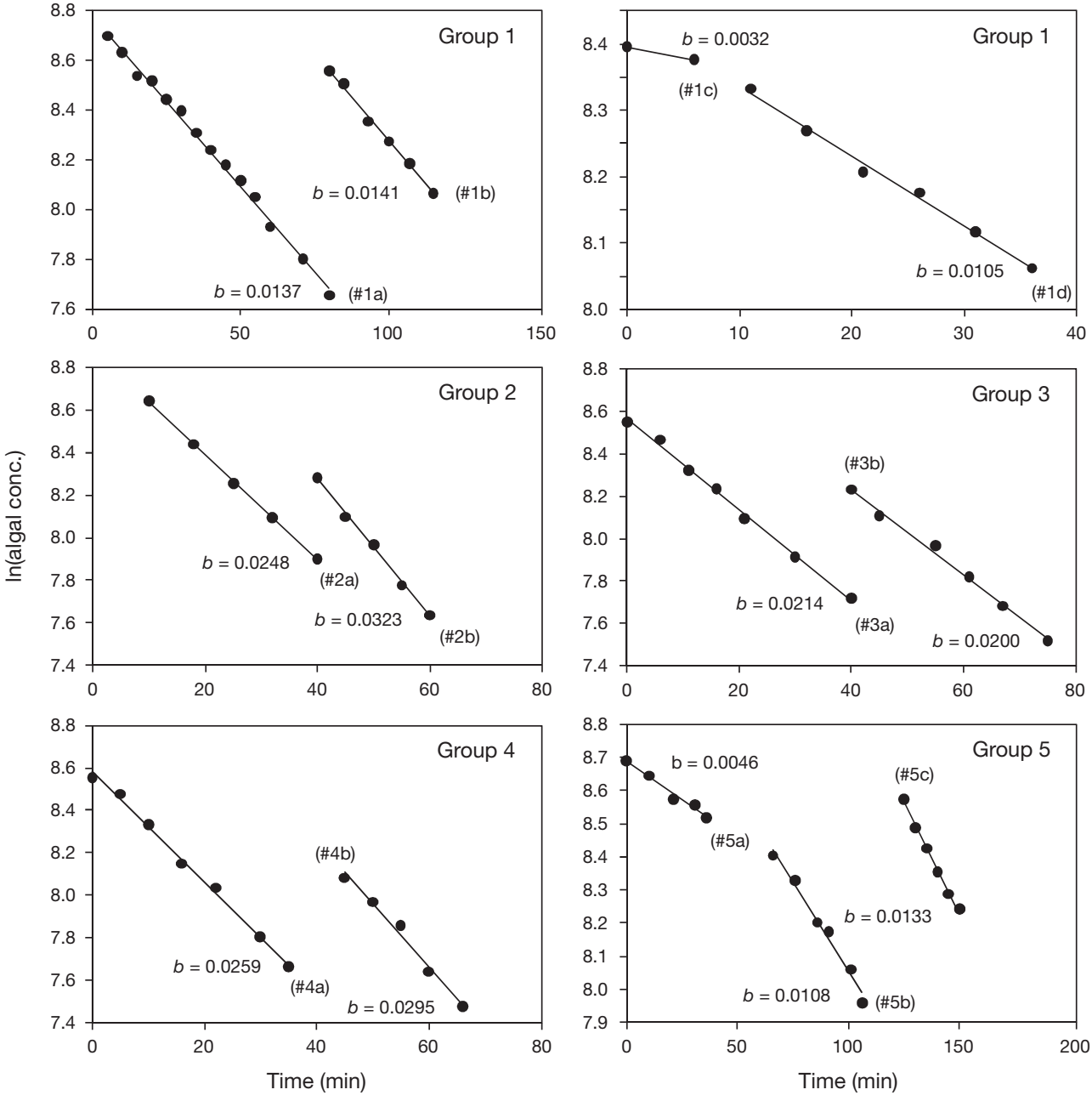

Fig. 2. *Mytilus edulis*. Clearance rate experiment samples from the 5 shell sizes of mussels (Table 1). The slope *b* of the linear regression line for each experiment, started from 10 to 60 min after addition of algal cells to the tank, is shown

tration of algal cells (C) and filtration rate (F) found from clearance measurements at each position (z) of the laser sheet, as well as the water temperature (T).

In the example of a single recorded particle image (Fig. 15A), the seeding particles appear as bright spots and the exhalant aperture and part of the shell can be seen to the lower right. The velocity vector field (Fig. 15B) shows the coordinate system and the extent of the field while the contour plot of turbulent kinetic energy ($k \approx 0.75$ [<uu> + <vv>], Fig. 15C) illustrates the well-defined shear layers bounding the spreading exhalant jet.

The profiles of axial velocity V_x across the jet at the distance x = 5.0 mm from the exhalant aperture are shown for experiment #503 in Fig. 16. It can clearly be seen that the velocity is greatest at the centre plane (z = 0 mm) and then decreases in off-centre planes. The exhalant opening along the major axis

Table 1. *Mytilus edulis*. Individual filtration rate (F) calculated from clearance rate experiments. V = water volume in tank, n = number of mussels in tank, L = shell length (mean ± SD), W = body dry weight (mean ± SD), CI = condition index (mean ± SD), b = slope of regression line in clearance rate experiment (Fig. 2). [a]Maximum filtration rate values used in Table 2, [b]reduced filtration rate values used in Table 3

Experiment #	V (l)	n	L (mm)	W (g)	CI (g cm^{-3})	b (min^{-1})	F (ml min^{-1})	F (l h^{-1})
1a	24	2	85.2 ± 0.1	2.85 ± 1.380	4.6 ± 2.2	0.0137	164	9.84
1b	24	2	85.2 ± 0.1	2.85 ± 1.380	4.6 ± 2.2	0.0141	169	10.14
1c	48	2	82.6 ± 3.0	2.78 ± 0.712	4.9 ± 0.7	0.0032	77	4.62[b]
1d	48	2	82.6 ± 3.0	2.78 ± 0.712	4.9 ± 0.7	0.0105	252	15.12[a]
2a	9	2	63.8 ± 0.2	1.88 ± 0.193	7.2 ± 0.8	0.0248	112	6.72
2b	9	2	63.8 ± 0.2	1.88 ± 0.193	7.2 ± 0.8	0.0323	145	8.70[a]
3a	14	4	49.3 ± 0.6	0.74 ± 0.091	6.2 ± 0.8	0.0214	75	4.50[a]
3b	14	4	49.3 ± 0.6	0.74 ± 0.091	6.2 ± 0.8	0.0200	70	4.20
4a	4	4	26.1 ± 0.6	0.08 ± 0.016	4.7 ± 0.5	0.0259	26	1.56[b]
4b	4	4	26.1 ± 0.6	0.08 ± 0.016	4.7 ± 0.5	0.0295	30	1.80[a]
5a	1.5	4	16.0 ± 0.4	0.03 ± 0.004	6.2 ± 0.7	0.0046	2	0.12[b]
5b	1.5	4	16.0 ± 0.4	0.03 ± 0.004	6.2 ± 0.7	0.0108	4	0.24
5c	1.5	4	16.0 ± 0.4	0.03 ± 0.004	6.2 ± 0.7	0.0133	5	0.30[a]

Table 2. *Mytilus edulis*. Shell length (L), body dry weight (W), condition index (CI), gill area (G), maximum filtration rate (F_{max}), exhalant siphon cross-sectional area (ESA), shell opening degree (SOD), and estimated velocity of exhalant jet ($V_e = F/ESA$). Means ± SD; n = 2 to 9. [a]estimated from ESA Method 1; [b]estimated from ESA Method 2

Experiment #	F_{max} (l h^{-1})	G (cm^2)	ESA^a (cm^2)	ESA^b (cm^2)	SOD (mm)	V_e^a (cm s^{-1})	V_e^b (cm s^{-1})
1d	15.1	88.6 ± 5.0	0.519 ± 0.133	0.582 ± 0.159	9.2 ± 1.2	8.1	7.2
2b	8.7	52.6 ± 0.6	0.241 ± 0.020	0.265 ± 0.032	6.0 ± 0.9	10.0	9.1
3a	4.5	28.8 ± 3.0	0.128 ± 0.011	0.197 ± 0.041	4.2 ± 0.3	9.8	6.3
4b	1.8	6.3 ± 0.4	0.086 ± 0.022	0.105 ± 0.029	3.3 ± 0.4	5.7	4.7
5c	0.3	3.5 ± 0.7	0.011 ± 0.003	0.019 ± 0.0001	2.8 ± 1.0	7.8	4.5
					Mean ± SD	8.3 ± 1.7	6.4 ± 1.9

Table 3. *Mytilus edulis*. Experimentally measured reduced filtration rate (F_{red}), exhalant siphon area (ESA), shell opening degree (SOD), estimated velocity of exhalant jet ($V_e = F/ESA$). Percentage reduction compared to maximum value is indicated in brackets. [a]Estimated from ESA Method 1.

Experiment #	F_{red} (l h^{-1})	ESA^a (cm^2)	SOD (mm)	V_e^a (cm s^{-1})
1c	4.62 (31)	0.342 (66)	7.35 (80)	3.8 (46)
4a	1.56 (88)	0.079 (92)	2.67 (81)	5.5 (96)
5a	0.12 (46)	0.009 (82)	1.70 (61)	3.6 (57)
			Mean ± SD	4.3 ± 1.0

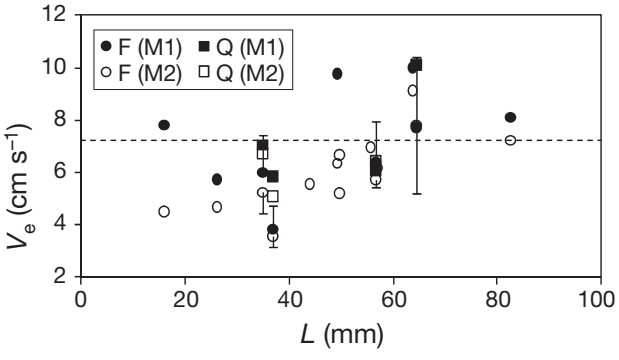

Fig. 3. *Mytilus edulis*. Exhalant jet velocity (V_e) as a function of shell length (L), calculated from clearance rate (F) and PIV flow rate (Q) measurements using siphon area (ESA) determined by 2 methods (M1, M2, Table 5). Multiple measurements (n = 2 to 5) were made on 35.0, 38.6, 56.6, and 64.5 mm mussels, and for these individuals mean ± SD is plotted. The ratio of 'model equation' $F = 0.0022L^2$ (Fig. 7) and 'model equation' $ESA = 0.000085L^2$ (Fig. 10), which expresses the 'model jet velocity' V_e = 7.2 cm s^{-1} is indicated as a dashed line. This value should however be increased by 15% to 8.3 cm s^{-1} due to a reduction in effective ESA (see main text)

has a cross section that is not symmetrical, so that the centre is not well defined but rather judged by eye during the positioning of the laser sheet. For the centre plane (z = 0 mm), profiles of V_x and transversal velocity (V_y) at axial positions along the jet from x = 5 to 15 mm are shown in Fig. 17. The change of these profiles with downstream distance (due to viscous diffusion and entrainment) illustrates the spreading of

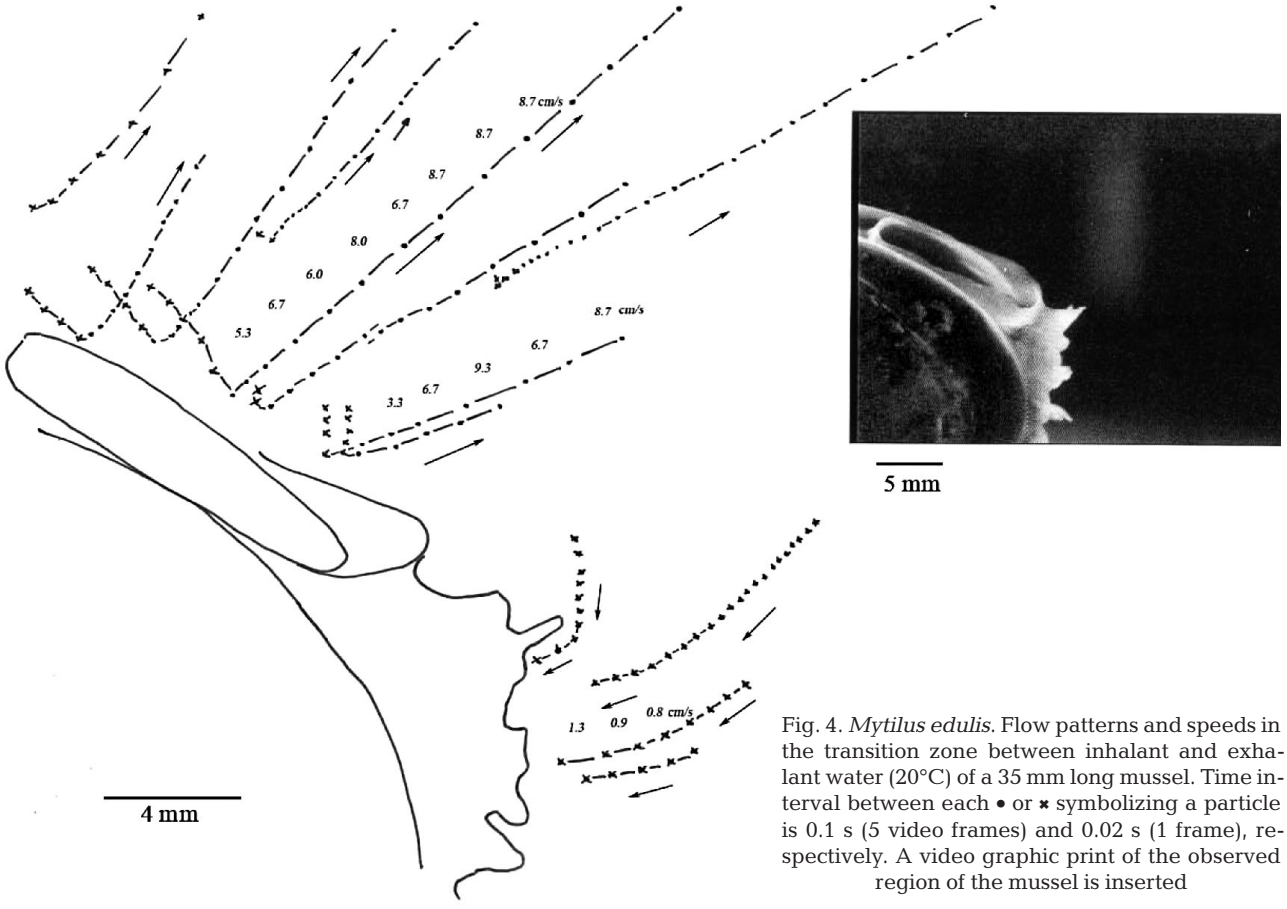

Fig. 4. *Mytilus edulis*. Flow patterns and speeds in the transition zone between inhalant and exhalant water (20°C) of a 35 mm long mussel. Time interval between each • or × symbolizing a particle is 0.1 s (5 video frames) and 0.02 s (1 frame), respectively. A video graphic print of the observed region of the mussel is inserted

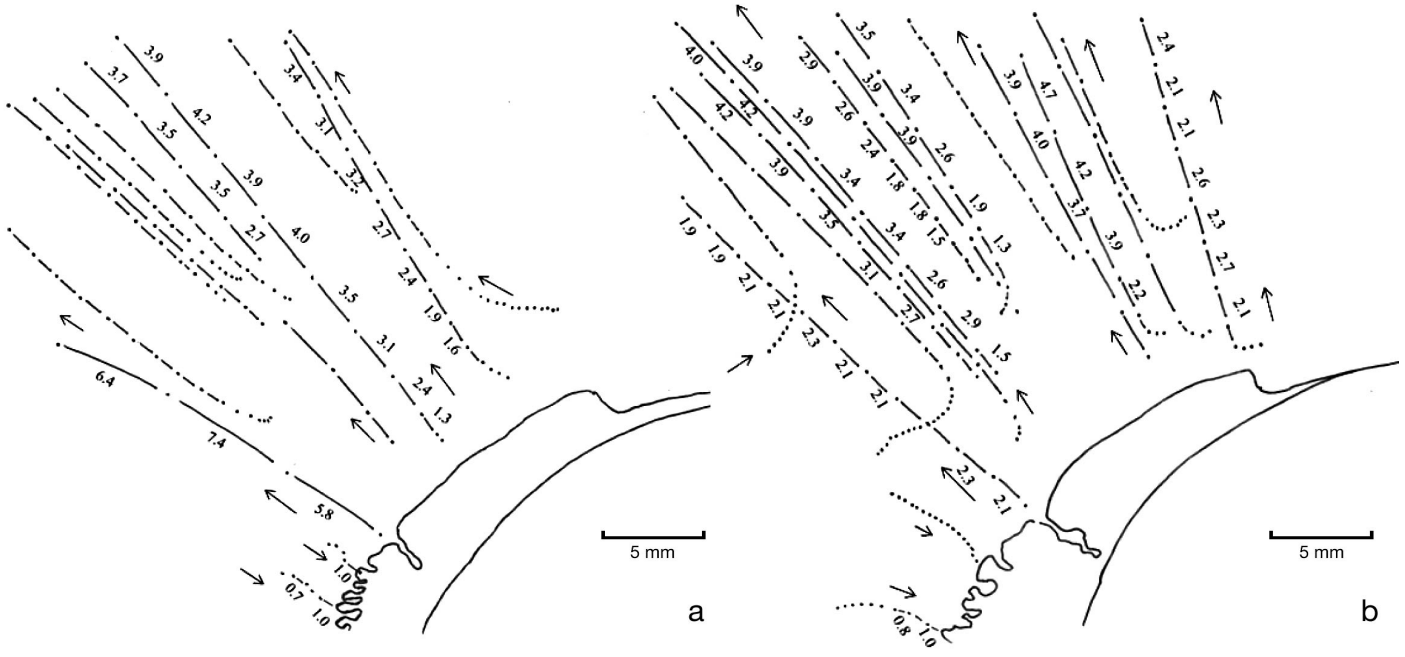

Fig. 5. *Mytilus edulis*. Flow patterns and speeds in the transition zone between (a) inhalant and (b) exhalant water (12°C) of a 56 mm long mussel. Time interval between each dot symbolizing a particle is 0.1 s (5 video frames)

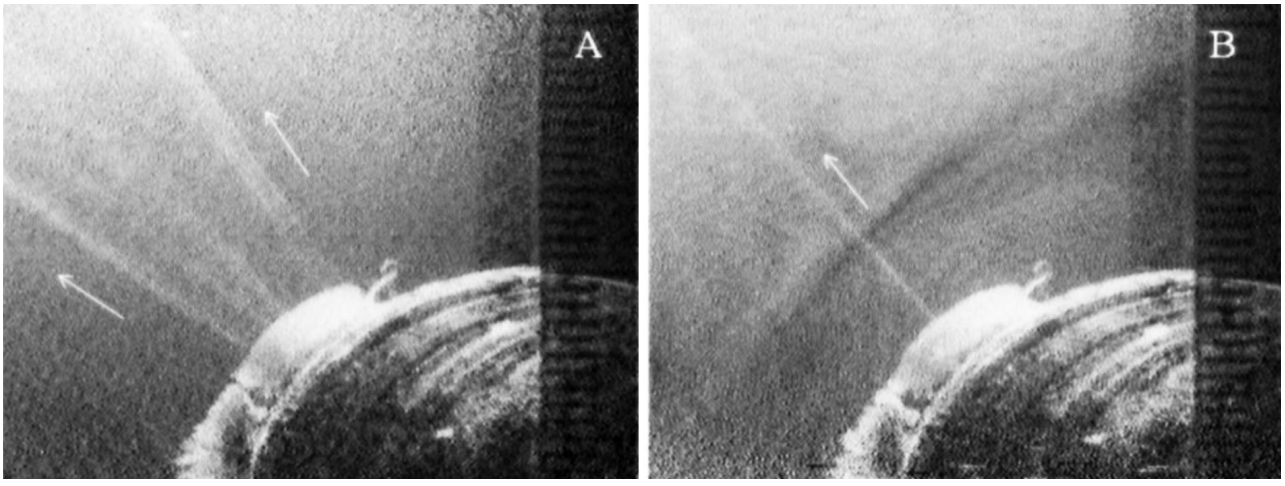

Fig. 6. *Mytilus edulis*. Video graphic prints of visualized (fluorescein) exhalant jets from a 56 mm long mussel (12°C). (A) The whole exhalant jet is seen indicating the spreading of the jet. (B) Only a thin ray of the jet is seen because the dye entered the inhalant opening as a very thin streak from the dosing-pipette tip. Right side: mm scale

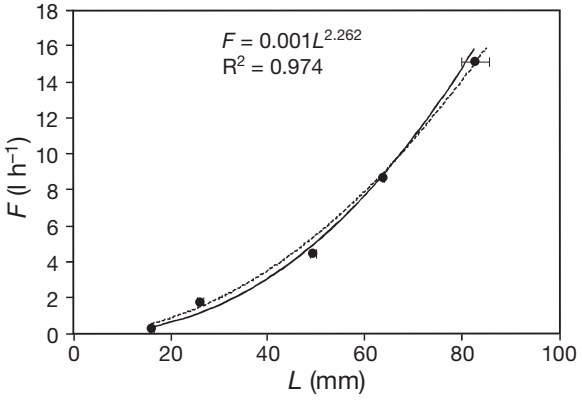

Fig. 7. *Mytilus edulis*. Maximum measured filtration rate (*F*) (11.6°C) as a function of mean (± SD) shell length. Formula for dashed line ('model equation'): $F = 0.0022L^2$

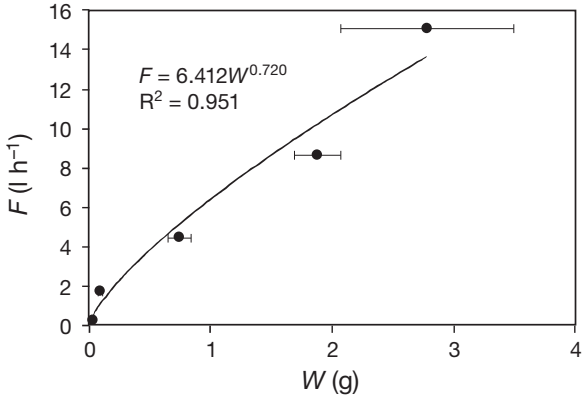

Fig. 9. *Mytilus edulis*. Filtration rate (*F*) (11.6°C) as a function of mean (± SD) body dry weight (*W*)

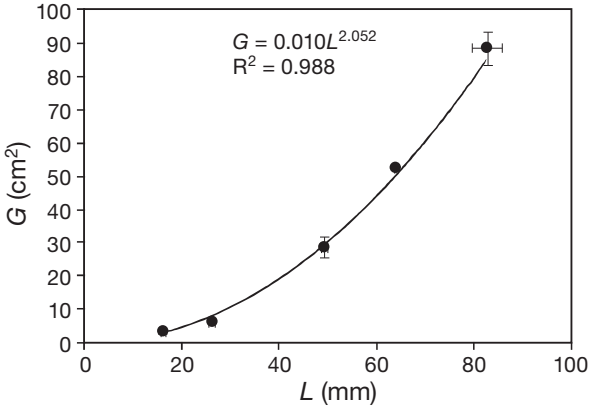

Fig. 8. *Mytilus edulis*. Gill area (*G*) as a function of shell length. All means ± SD

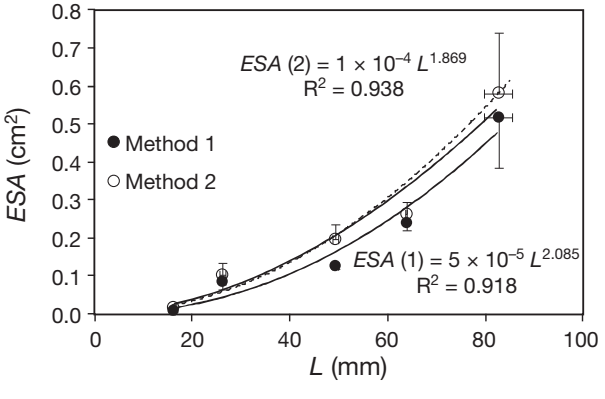

Fig. 10. *Mytilus edulis*. Exhalant siphon area (*ESA*) estimated by 2 methods as a function of shell length (*L*). All means ± SD. Formula for dashed line ('model equation'): $ESA = 0.000085L^2$

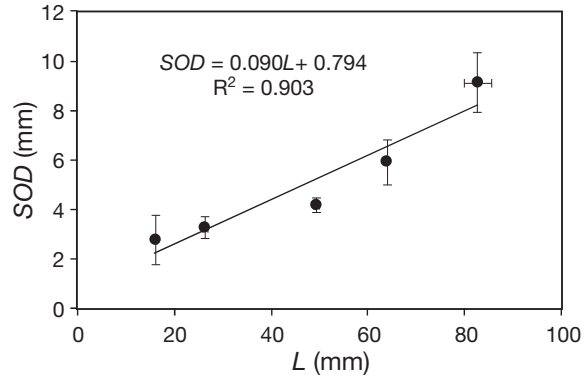

Fig. 11. *Mytilus edulis*. Shell opening degree (*SOD*) as a function of shell length (*L*), all means ± SD

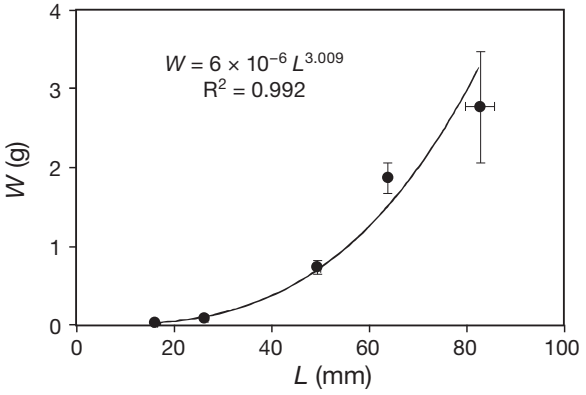

Fig. 12. *Mytilus edulis*. body dry weight (*W*) as a function of shell length (*L*), all means ± SD

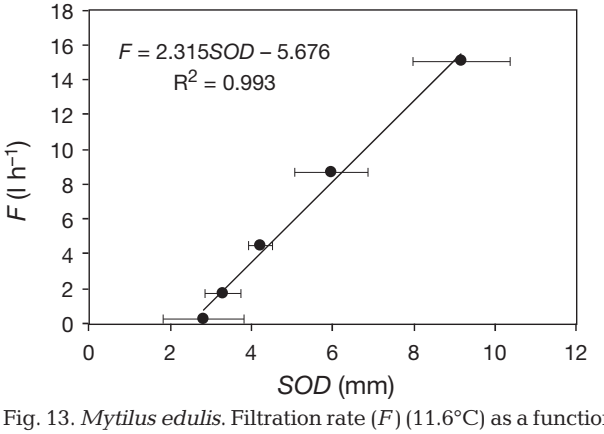

Fig. 13. *Mytilus edulis*. Filtration rate (*F*) (11.6°C) as a function of shell opening degree (mean ± SD)

the jet. Nevertheless, the axial velocity measured closest to the aperture at $x = 5.0$ mm would be a good estimate of the velocity at the aperture.

The flow rate (Q) in the jet at $x = 5$ mm for a given mussel was estimated by integrating the velocity from the 5 measured V_x profiles over the cross sectional area of the jet. Each profile was taken to correspond to a layer of thickness 1.0 mm and the integration extended from $y = -10.0$ to $+10.0$ mm. Table 5 lists this flow rate for each of the 4 shell lengths of mussels (#502 to #505) as well as the filtration rates (F) obtained from clearance measurements. With the exception of experiment #504, the deviation between results obtained by the 2 methods is <26% and may be ascribed to the fact that integration will include some entrainment flow. By inspection of Fig. 16 the exhalant jet velocity is seen to be above 8 cm s^{-1} over most of the mid-plane.

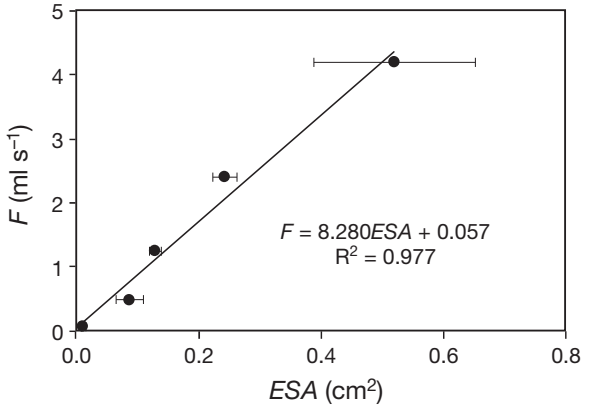

Fig. 14. *Mytilus edulis*. Filtration rate (*F*) (11.6°C) as a function of exhalant siphon cross-sectional area (*ESA*, mean ± SD) measured by Method 1

Table 4. *Mytilus edulis*. Data from PIV experiment #503 (= logbook number) for $L = 56.6$ mm shell length mussel. C = algal concentration, F = filtration rate, z = lateral position, Temp. = water temperature.

Expt #	C (cells ml^{-1})	F (ml min^{-1})	z (mm)	Temp. (°C)
503-01	3948	151.1	0.0	16.8
503-02	4151	166.4	1.0	17.3
503-03	3743	141.9	2.0	17.3
503-04	3093	153.3	–1.0	17.3
503-05	3093	153.3	–2.0	17.3

The exhalant jet expands and slows down gradually with distance due to entrainment of the surrounding water. The rate of expansion can be estimated from the angle between the x-axis and the velocity vector (V_x, V_y) in the centre plane ($z = 0$ mm). At $x = 5$ mm, using values from Fig. 17 gives half angles of approximately arctan(2.8 cm s^{-1} / 10.0 cm s^{-1}) = 15.6° in the left, and arctan(1 cm s^{-1} / 10.0 cm s^{-1}) = 5.7° in the right half-plane, hence an average of 10.7°. For comparison, the spreading of the jet visualized by flourescein (Fig. 6A) and that suggested by regions of high turbulent kinetic energy in the shear layers (Fig. 15C) both indicate a half-angle of 9.5°.

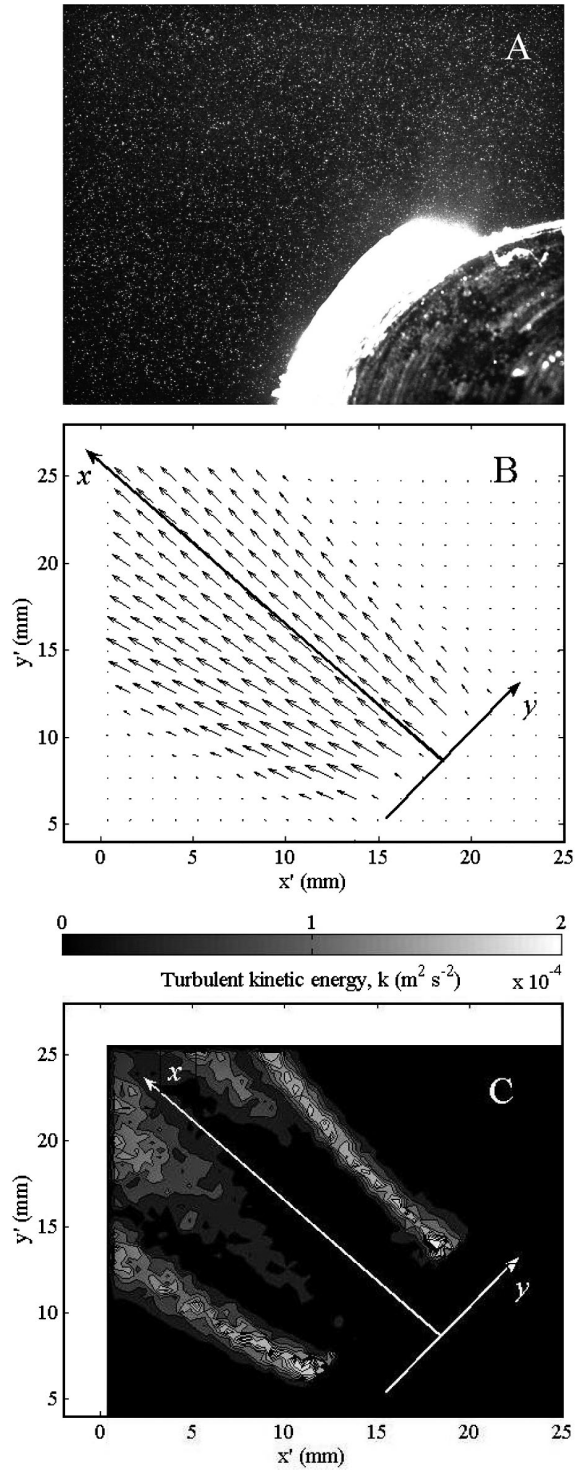

Fig. 15. *Mytilus edulis*. (A) Particle image velocimetry image of captured field (32 × 25.5 mm) showing seeding particles in the jet flow, the exhalant siphon and part of the shell to the lower right. (B) Averaged vector field of the exhalant jet of experiment #503 (only every third vector is shown for clarity). (C) Contour plot of turbulent kinetic energy, $k \approx 0.75$ (<uu> + <vv>), (excluding noisy region near aperture) showing jet spreading by shear layers

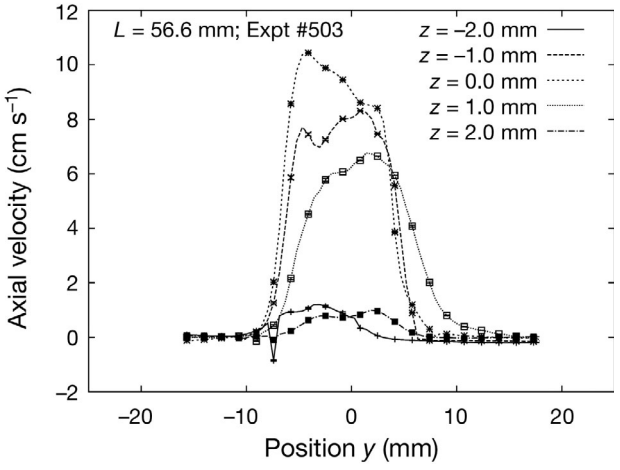

Fig. 16. *Mytilus edulis*. Velocity profiles $V_x(y)$ at 5 z-positions through the exhalant jet at a distance x = 5.0 mm from the exhalant aperture

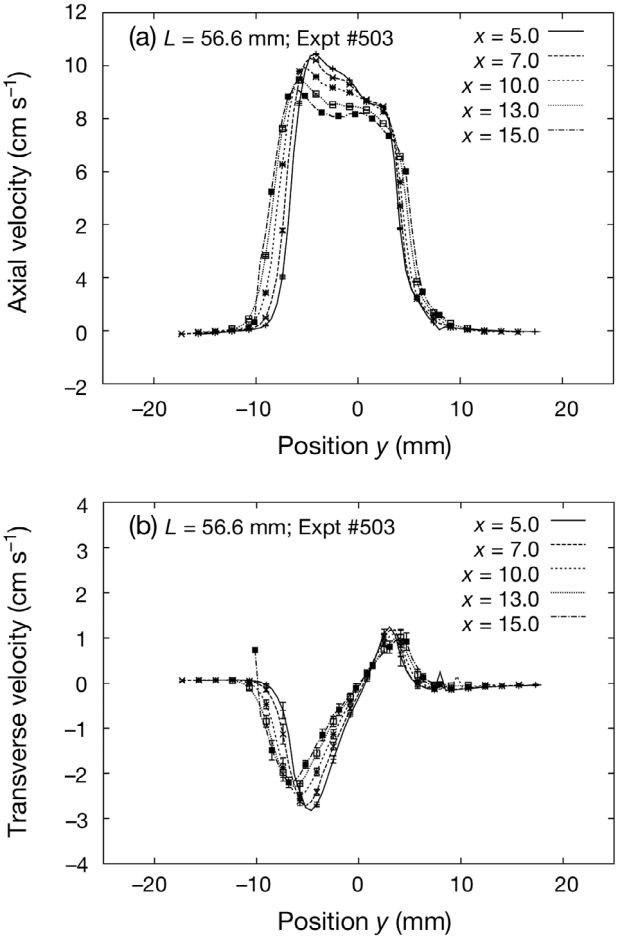

Fig. 17. *Mytilus edulis*. Velocity profiles $V_x(y)$ (a) and $V_y(y)$ (b) at 5 x-positions from the exhalant aperture. The profiles are shown for the center plane (z = 0 mm) at the middle of the exhalant jet. The error bars show ± 2SD

Table 5. *Mytilus edulis*. Velocity of exhalant jet (V_e) calculated from exhalent siphon area (*ESA*), filtration rate (F) from clearance rate experiments, and flow rate (Q) from PIV measurements (experiments #502 to #505). [a]Estimated from *ESA* Method 1; [b]estimated from *ESA* Method 2

L (mm)	ESA^a (cm^2)	ESA^b (cm^2)	Q (ml min^{-1})	F (ml min^{-1})	V_e^a (Q) (cm s^{-1})	V_e^b (Q) (cm s^{-1})	V_e^a (F) (cm s^{-1})	V_e^b (F) (cm s^{-1})
82.6	0.519	0.582		252.0			8.1	7.2
63.8	0.241	0.265		145.0			10.0	9.1
49.3	0.128	0.197		75.0			9.8	6.3
26.1	0.086	0.105		29.5			5.7	4.7
16.0	0.011	0.019		5.0			7.8	4.5
64.5	0.328	0.327	198.6 (#502)	211.5	10.1	10.1	10.7	10.8
64.5	0.487	0.467		168.2			5.8	6.0
64.5	0.433	0.437		173.9			6.7	6.6
56.6	0.459	0.434	167.5 (#503)	143.6	6.1	6.4	5.2	5.5
56.6	0.357	0.454		160.7			7.5	5.9
36.8	0.304	0.350	106.4 (#504)	81.2	5.8	5.1	4.5	3.9
36.8	0.318	0.312		60.9			3.2	3.3
35.0	0.254	0.266	107.2 (#505)	83.6	7.0	6.7	5.5	5.2
35.0	0.246	0.283		85.4			5.8	5.0
35.0	0.291	0.322		86.2			4.9	4.5
35.0	0.159	0.168		49.3			5.2	4.9
35.0	0.134	0.175		68.4			8.5	6.5
49.7		0.274		85.4				5.2
49.7		0.213		85.4				6.7
44.0		0.198		65.8				5.5
55.7		0.261		108.9				7.0
57.0		0.310		114.4				6.2

DISCUSSION

Allometric equations and scaling

The experimentally measured filtration rate (F) and gill area (G) are both near proportional to the square of the shell length (L), i.e. $F = aL^2$ (cf. Fig. 7) and $G = aL^2$ (cf. Fig. 8), and these expressions can therefore be used in future modelling of the blue mussel *Mytilus edulis*. Further, it was found that the body dry weight (W) is proportional to L^3 (Fig. 12), implying that L is proportional to $W^{1/3}$, so that $F = a(W^{1/3})^2 = aW^{2/3} = aW^{0.67}$ which is in good agreement with the actually determined exponent $b = 0.72$ (Fig. 9). It should, however, be remembered that the relationship between body weight and shell length (cf. the condition index, Table 2) is not constant, but varies from population to population and during the year due to spawning in spring, growth during summer, and starvation during winter (Dare 1976, Riisgård 2001a, Filgueira et al. 2008).

The equations for filtration rate as a function of shell length or body dry weight are in good agreement with the formulae mentioned by Riisgård (2001a, their Table 1). Thus, the filtration rate of *Mytilus edulis* as a function of shell length was measured by means of the 'suction' method by Kiørboe & Møhlenberg (1981) who found $F = 0.0012L^{2.14}$, which is nearly identical to the present equation (Fig. 7). Flow rates (Q) obtained by integration of PIV-velocity profiles are in fairly good agreement with filtration rates measured in clearance experiments (Table 5), and the exhalant jet velocities measured by PIV (Figs. 16 & 17) are in reasonably good agreement with the 'model jet velocity' of $V_e = 8.3$ mm s^{-1} (Fig. 3). Given the observed large spreading angle of the jet, a certain amount of discrepancy may be ascribed to entrainment of ambient fluid into the jet.

The effect of adding algal cells to the ambient water of unfed mussels (cf. Fig. 2) is a well described phenomenon (e.g. Riisgård & Randløv 1981, Newell et al. 2001, Riisgård et al. 2003, 2006) which in the present work was used to evaluate the effect of reduced shell opening degree on exhalant jet velocity (cf. 'reduced filtration rate values' in Tables 1 & 3). Compared with fully open mussels, the exhalant jet velocity was reduced in mussels with reduced shell opening degree (and smaller exhalant siphon cross-sectional area). Jørgensen et al. (1988) studied the relationship between 'passively controlled' (by means of a binding screw) and 'actively' (by the mussel) reduced shell opening degree, area of exhalant

siphon aperture, and filtration rate in *Mytilus edulis* of different sizes. It was found that the relations between shell opening (or siphon area) and filtration rates were similar for 'passively' and 'actively' controlled valve gape. For fully open *M. edulis*, Jørgensen et al. (1988, their Table 3) found that a filtration rate of 41 ± 3.6 ml min^{-1} was correlated with a siphon area of 12.9 ± 1.0 mm^2 (means ± SD), and thus the exhalant jet velocity was estimated at V_e = 41/12.9 = 5.3 cm s^{-1} which is comparable to, although slightly lower than, that estimated in the present work (Table 2). Jørgensen et al. (1988) concluded that reduced shell opening degree is correlated with retraction of the mantle edges and siphon, and that this results in a reduction in width of the gill-interfilament canals and thus in the distance between opposing bands of water-pumping lateral cilia, and further, that this distance is the main factor in determining the pump pressure and filtration rate in *M. edulis*.

For fully open *Mytilus edulis*, exhalant siphon area versus shell length scales approximately as $ESA \propto L^2$ (Fig. 10) and filtration rate (or pumping rate Q for 100% retention) scales as F or $Q \propto ESA \propto L^2$ (Fig. 14). Based on these observations the theory of geometric similarity may serve to show that the exhalant jet velocity is essentially independent of mussel shell length. To show this, consider the pump and system characteristics of a mussel subject to zero backpressure (e.g. Riisgård & Larsen 1995, their Fig. 1a), replotted schematically as pressure head versus scaled volume flow Q/L^2 (Fig. 18). In *M. edulis* the pump characteristic of the leaky viscous ciliary pump follows a linear decrease of pressure head delivered with increasing volume flow (pumping rate) (Jørgensen et al. 1986, their Fig. 3):

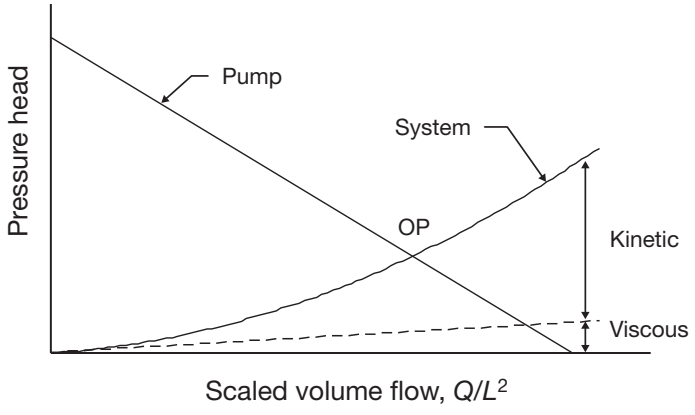

Fig. 18. Schematic of *Mytilus edulis* pump and system characteristics intersecting at the normal operating point OP. System characteristic is sum of linear viscous and quadratic kinetic resistances

$$\Delta p = \Delta p_0 (1 - Q/Q_{max}) = \Delta p_0 [1 - (Q/L^2)/(Q_{max}/L^2)] \quad (7)$$

The maximal (so-called shutoff) pressure head at zero flow (Δp_0) is essentially independent of shell length of mussel over a considerable range of larger sizes since the ciliary pump is generic in terms of basic pump units, consisting of approximately (Jones et al. 1992) identical gill-filaments with water pumping lateral cilia of the same length and with a beat frequency independent of shell length (i.e. area-specific pumping rate of the gills is independent of mussel shell length; same exponent $b \approx 2$ for F and G as a function of L, see Figs. 7 & 8). Therefore, the maximal volume flow (Q_{max}, at zero pressure head) is assumed to scale by shell length according to area of gills, i.e. $Q_{max}/L^2 \approx$ constant. As a consequence, pump characteristics for mussels of different shell length would all fall on the same line in a plot of pressure rise versus Q/L^2, as shown in the schematic Fig. 18.

The system characteristic is the sum of a linear contribution from viscous flow resistance and a quadratic contribution from the so-called kinetic loss due to the exhalant jet flow. The main contribution to the former (about 1/3 of the total pressure drop according to the example of Jørgensen et al. 1986, their Table 3) stems from the viscous flow through the gill-interfilamental canals. Treated as flow between parallel plates of generic (i.e. constant) spacing λ_{ifc} and length L_{ifc}, the frictional pressure drop is:

$$\Delta p_f = 12\mu L_{ifc} u_{ifc}/\lambda_{ifc}^2 \propto Q/L^2 \quad (8)$$

where the interfilamental water velocity is directly proportional to the ratio of volume flow to gill area, hence the scaling $u_{ifc} \propto Q/L^2$. The latter contribution (about half of the total) is the kinetic energy loss in the exhalant jet flow:

$$\Delta p_{kin} = \tfrac{1}{2}\rho V_e^2 \propto (Q/L^2)^2 \quad (9)$$

where the exit velocity equals the ratio of volume flow to exhalant opening area, hence the scaling $V_e \propto Q/L^2$. The remaining contributions (about 1/6 of the total) come from minor losses of inhalant flow and viscous resistance in the boundary layers in the flow from mantel cavity out through the exhalant opening. These contributions probably scale less well with relevant velocities as Q/L^2.

From the foregoing considerations it follows that the operating points of *Mytilus edulis* of different shell length will coincide in the scaled plot of characteristics in Fig. 18, hence specifically the magnitude of the kinetic head loss will be the same and consequently also the exit velocity V_e from the exhalant opening.

Exhalant jet velocity

The velocity of the exhalant jet has been studied by 3 methods for fully open mussels. Mean values of velocity were obtained indirectly from measured clearance rate divided by aperture area (V_e = 8.3 ± 1.7 cm s^{-1}, Method 1, Table 2), which are of the same order of magnitude as directly observed local velocities by particle tracking (up to 8.7 cm s^{-1}) and particle image velocimetry (~ 8.6 to 11.1 cm s^{-1}). All available data on V_e obtained in clearance and PIV measurements are placed together in Table 5 and depicted in Fig. 3 along with the 'model jet velocity' found as the ratio of 'model equation' for F (Fig. 7) and the 'model equation' for ESA (Fig. 10): $V_e = F/ESA$ = 7.2 cm s^{-1}, which may be used as a shell length independent constant in future modelling. This value should, however, be increased by ~15% to 8.3 cm s^{-1} due to a reduction in effective ESA (see below). The lower mean values obtained by area Method 2 deserve an explanation. In Method 1, the area of the oval aperture is underestimated due to its more rectangular than elliptical shape, giving a high value of velocity, which fortuitously proves to be a good estimate. In Method 2, the area is probably quite accurate, but to use this it should be taken into consideration that flow from the large mantel cavity into the exhalant siphon involves the formation of thin viscous boundary layers along the walls such that the velocity distribution in the jet leaving at the aperture consists of a core of rather uniform velocity V_0 surrounded by boundary layers in which the velocity drops to zero. Thus the effective area for estimating the mean jet velocity V_e is the actual area minus the perimeter of the aperture multiplied by the displacement boundary layer thickness, δ_1, which may be evaluated approximately as for flat plate flow from (Schlichting 1979, p. 141 therein),

$$\delta_1 = 1.72\ (\nu L_s/V_0)^{1/2} \quad (10)$$

where ν (= 0.01 cm^2 s^{-1}) is the kinematic viscosity of seawater and L_s (≈ 0.2 cm) the length of the siphon. Taking V_0 ≈ 8 cm s^{-1} gives δ_1 = 0.027 cm and, for experiment 1d of Table 2, this leads to a reduction in effective area of ~15%, so Method 2 would more correctly lead to V_e = 8.28 cm s^{-1}, which is in good agreement with the other results. Hence, in accord with the derived scaling laws, it is concluded that the exhalant jet speed for fully open mussels is approximately independent of shell length, in agreement with the scaling derived.

To help the development of models for biomixing (cf. Larsen & Riisgård 1997) due to exhalant jets from mussels, possibly aiding the supply of food particles by turbulent mixing, it is of importance to know the kinetic energy flow delivered by such jets to the ambient water. But as a consequence of the non-uniform velocity distribution emerging from natural apertures, as found in the present study (Figs. 16 & 17) and by Troost et al. (2009), it is not possible to estimate the momentum and kinetic energy of the exhalant jet given only volume flow F and aperture area ESA, hence mean velocity $V_{x,m}$ (= F/ESA). For the ideal case of a perfectly flat velocity profile at $V_{x,m}$, the flow of momentum and kinetic energy per unit mass are simply $V_{x,m}F$ and $\frac{1}{2}V_{x,m}^2F$, respectively. Correct results, obtained by integration of measured profiles of experiment #503 over the aperture may be written as $C_2V_{x,m}F$ and $C_3\frac{1}{2}V_{x,m}^2F$, respectively, where we find the correction factor to be C_2 = 1.4 and C_3 = 2.2, respectively, at x = 5 mm, which illustrates the magnitude of corrections to be expected. It is also of interest to note the measured levels of turbulent kinetic energy in the shear layers of the jet (Fig. 15C) of up to ~2 ×10^{-4} m^2 s^{-2}. Although this is no indication of the turbulence level in the far field (not studied), it is noted that Wiles et al. (2006, their Fig. 5) measured similar levels 2 to 3 cm above mussels at low wave height that produced less turbulence.

The velocities of the exhalant jet obtained in the present study (Figs. 3, 16 & 17) may be compared to those recorded in recent studies by Stamhuis (2006), Maire et al. (2007), Frank et al. (2008), MacDonald et al. (2009), and Troost et al. (2009). Using PIV, Stamhuis (2006) measured the exhalant velocity in *Mytilus edulis* to be only ~0.5 cm s^{-1}. Maire et al. (2007, their Fig. 8A) measured the maximal velocity of exhalant water in *Mytilus galloprovinciales* using a hot-film probe, and the maximal velocities were between 3.30 and 4.60 cm s^{-1} when the probe was placed 2 mm from the aperture in the axis of the centre of the exhalant siphon. Frank et al. (2008) reported average velocities of 4.32 ± 0.39 cm s^{-1} (mean ± SD) and a maximum velocity of 12.31 cm s^{-1} in one type of experiments ('animal-generated flow velocities'), whereas the average maximum excurrent velocities were found to range from 1.7 to 3.8 cm s^{-1} in another type of experiments ('mussel feeding study'). The filtration rate (or clearance rate) as a function of the exhalant siphon area has been measured for a 60 mm shell length *M. edulis* by MacDonald et al. (2009, their Fig. 3A). A suggested line for the relationship is F = 10 × ESA, and thus the velocity of the exhalant jet = slope of line = F (l h^{-1} g^{-1})/(10 × ESA (mm^2)) = 0.28 × F (cm^3 s^{-1})/(0.1 ESA (cm^2)) = 2.8 cm s^{-1}. Finally, the average exhalant jet velocity in *M. edulis* was calcu-

lated to be 18.5 cm s^{-1} by Troost et al. (2009) using an 'average' exhalant siphon cross-sectional area of 0.06 cm^2 for a mussel ~4.0 l h^{-1}. According to the present Fig. 7, a mussel with this filtration rate has a shell length of about 40 mm, and according to Fig. 10, the corresponding exhalant siphon cross-sectional area would be 0.1 cm^2, or ~1.6 times larger than the value used by Troost et al. (2009). Overall, the exhalant jet velocities in the present study are in fairly good agreement with both Frank et al. (2008) and Troost et al. (2009).

Velocity fields from particle image velocimetry

The central 3 velocity profiles (at z = –1, 0 and +1 mm) of Fig. 16 cover the major part of the area of the oval exhalant aperture (Fig. 1C) ($2a \approx 10$ mm, $2b \approx 3$ mm) and show axial jet velocities in the range from 6 to 11 cm s^{-1}, with a mean value of ~8 cm s^{-1} that is in good agreement with the other results. Note that the 0.5 mm thick laser sheet at positions $z = -2$ and +2 mm barely captures the low velocities at the edge of the oval jet. Although recorded close to the aperture (x = 5 mm), the profiles in Fig. 16 show thick boundary layers arising from entrainment that continue to increase in thickness downstream (Fig. 17 a), suggesting rapid spreading of the jet. The spreading half-angle of ~9.5° observed from fluorescein-visualization (Fig. 6A) and turbulence in shear layers (Fig. 15C) far exceeds what is found in round jets (Kwon & Seo 2005, their Fig. 9). Here, for Reynolds number Re <437 and x/d <20, the spreading rate in terms of change in radius (r) with axial position (x) of a round jet is ~$dr/dx \approx 2/70$, corresponding to a half-angle of ~1.6°.

Another issue is the complex shape of the velocity profiles (Fig. 16). Profiles of axial velocity V_x tend to a 'top-hat' shape bounded by boundary layers developed in the contraction flow from mantel cavity out through the exhalant siphon and further diffused into the ambient through the process of entrainment. Yet, profiles are asymmetric with higher values at negative y-values corresponding to the side of the aperture of larger width (Fig. 1C), which is to be expected. A similar effect was observed by Frank et al. (2008), however, for flow from an aperture with 2 regions of large width separated by 1 region of narrow width, leading to a so-called bifurcated (double peaked) jet. It is thus not meaningful to treat the initial jet as a perfect flat top-hat profile, nor as developed Poiseuille flow from a circular duct as done by Maire et al. (2007) who assumed an average velocity being half of the maximal velocity, which was measured with a hot-film probe in the center of the exhaled jet. Rather, to model the flow near a mussel, one should solve the complete problem of flow from the mantel cavity through the exhalant siphon to generate a realistic asymmetric jet as observed. Yet, preliminary computational studies of jet spreading and penetration have been performed using the approximate profiles shown in Fig. 19 for experiment #503. Thus, we have fitted the V_x-velocity profile closest to the exhalant aperture to a profile composed of parabolic functions at the sides and a core of constant velocity in the middle. This is close to the expected flow produced by the reduction from the large exhalant suprabranchial cavity into the short exhalant siphon thus emulating the exhalant flow of the mussel. The result shown in Fig. 19 (a) is based on the profile,

$$V_x(y) = [V_0/(y_1 - y_0)^2]\,[y_0^2 - y^2 + 2y_1(y - y_0)],\ y_0 < y < y_1 \quad (11a)$$

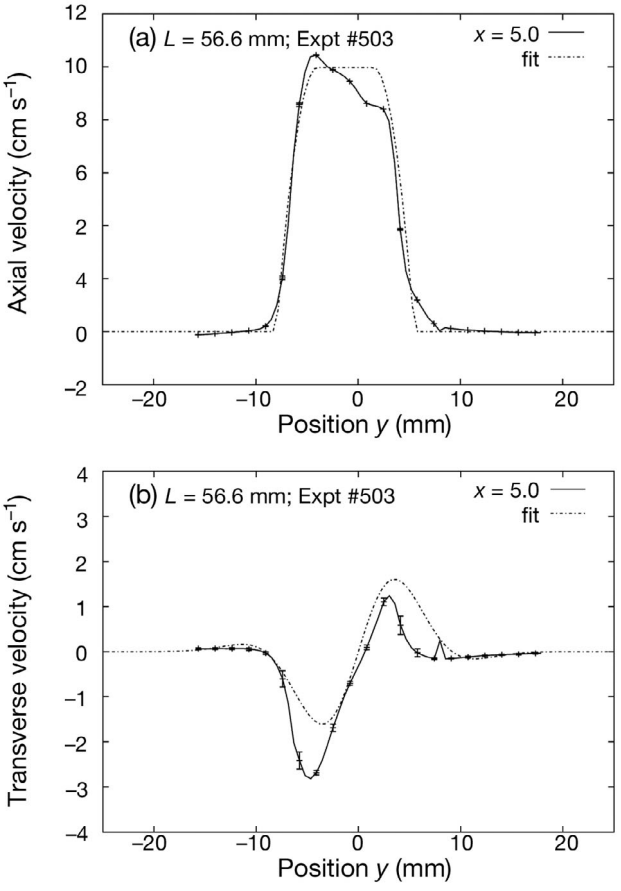

Fig. 19. *Mytilus edulis*. Measured velocity profiles (solid) compared to fitted profiles (dashed, from Eqs. 11 & 12) at the center plane (z = 0 mm) at distance x = 5.0 mm from the exhalant aperture, (a) axial velocity $V_x(y)$ and (b) transverse velocity $V_y(y) \pm 2$ SD

$$V_x(y) = V_0,\ y_1 < y < y_2 \quad (11b)$$

$$V_x(y) = [V_0/(y_3 - y_2)^2]\,[y_3^2 - y^2 + 2y_2(y - y_3)],\ y_2 < y < y_3 \quad (11c)$$

where $y_0 = -8.0$ mm, $y_1 = -4.0$ mm, $y_2 = 1.5$ mm, $y_3 = 5.5$ mm, and $V_0 = 10.0$ cm s^{-1}.

The transverse V_y-velocity from the same experiment has been fitted to a function resembling the one of the jet flow originating from a point source (Schlichting 1979, p. 232 therein), implying a decay of form $\exp(-y^2/s^2)$ outside the core of the jet:

$$V_y(y) = \exp(y^2/s^2)\,[ey - (h/4)y^3]/[1 + (g/4)y^2]^2 \quad (12)$$

where $e = 7.40$ s^{-1}, $h = 35.4$ s^{-1} cm^{-2}, $g = 0.1065$ cm^{-2}, and $s = 0.628$ cm. The resulting profile is shown in Fig. 19a.

Judging by the above profiles, the mean spreading angle of the jet is of the order 10.7°. Preliminary, full 3-dimensional unsteady Large Eddy Simulation (LES) for a round jet with a parabolic starting profile and Reynolds number (Re) 400 (not published) have resulted in a spreading angle of 4.6°, which bears some resemblance to the experimental results of Kwon & Seo (2005, their Fig. 4) for a round jet from a nozzle with some flow development at Re = 437. However, other LES results utilizing a starting velocity profile with a potential core and boundary layers (similar to Fig. 19b) have given a spreading angle of 9.6°. Nevertheless, more realistic results require the consideration of the actual oval shape of the exhalant aperture, because jets from e.g. elliptical nozzles are quite different from jets from circular nozzles in terms of stability, entrainment and spreading rate. Thus, the instability of shear layers in elliptical jets is characterized by spatial disturbances that grow faster in the direction of the minor compared to the major axis (Crighton 1973). This supports the observation that the spreading rate is higher in the same direction of the minor axis, implying that a cross-over of axis (axes-switching) takes place downstream (Hussain & Husain 1989, their Fig. 4) such that the elliptical shape tends to become perpendicular to the original orientation. This phenomenon has also been demonstrated by simple potential flow theory (without viscosity and surface tension) for a liquid jet falling under the influence of gravity from an elliptical orifice, as well as from an egg-shaped orifice (Geer & Strikwerda 1980, their Figs. 2 & 6). The present PIV-results — aimed at determining the velocity at the exit of the exhalant siphon— cover only a short downstream distance of 5 diameters of the jet; hence do not reveal the foregoing complex phenomena. It remains to demonstrate, by computational means, how such phenomena influence the flow and feeding conditions for individual as well as groups of mussels.

Another aspect of flow around mussels that has not been examined here is the 'jet in cross-flow' problem of a vertical exhalant jet being deflected by a horizontal current. This was studied by Ertman & Jumars (1988) who estimated the excurrent velocity of the cockle *Clinocardium nuttallii* to be 9 to 11 cm s^{-1} and observed an upwelling from the excurrent jet at the free surface of a flume, 13 cm above the bed at a free-stream velocity of 2.8 cm s^{-1}. Such high values of jet velocity were also observed by Price & Schiebe (1978) who, using a hot-film anemometer, measured excurrent siphon exit velocities of 11 to 14 cm s^{-1} for the freshwater clam *Anodonta* sp.

The present work has emphasized the crucial importance of studying fully open *Mytilus edulis* in terms of independently measured PTV, PIV, and filtration rate divided by exhalant aperture area, which were found to be in good agreement, showing that the exhalant jet velocity is near constant, at ~8 cm s^{-1}, and independent of shell length. Further, the PIV measurements have provided detailed velocity distributions inside the exhalant jet which is important information because computational modelling depends on such knowledge to provide boundary conditions for numerical flow models. Apart from such knowledge, it is also of importance to know the distance the exhalant jet can reach in the ambient water, and such measurements form part of ongoing experimental and modelling studies where the reported scaling laws in terms of mussel shell length are very useful tools.

Acknowledgements. We thank P. Buchhave for advice about optics, F. Willerval and C. Thouny for performing Large Eddy Simulations of a round jet, and J. T. Rasmussen for assisting with image processing. This work formed part of the MarBioShell project supported by the Danish Agency for Science, Technology and Innovation for the period January 2008 to December 2012.

LITERATURE CITED

André C, Jonsson PR, Lindegarth M (1993) Predation on settling bivalve larvae by benthic suspension feeders: the role of hydrodynamics. Mar Ecol Prog Ser 97:183–192

Angel DL, Eden N, Breitstein S, Yurman A, Katz T, Spanier E (2002) *In situ* biofiltration: a means to limit the dispersal of effluents from marine finfish cage aquaculture. Hydrobiologia 469:1–10

Butman CA, Frechette M, Geyer WR, Starczak VR (1994) Flume experiments on food supply to the blue mussel *Mytilus edulis* L. as a function of boundary–layer flow. Limnol Oceanogr 39:1755–1768

Clausen I, Riisgård HU (1996) Growth, filtration and respiration in the mussel *Mytilus edulis*: no regulation of the filter-pump to nutritional needs. Mar Ecol Prog Ser 141: 37–45

Coughlan J (1969) The estimation of filtering rate from the clearance of suspensions. Mar Biol 2:356–358

Crighton DG (1973) Instability of an elliptic jet. J Fluid Mech 59:665–672

Dare PJ (1976) Settlement, growth and production of the mussel, *Mytilus edulis* L., in Morecambe Bay, England. Fish Invest II 28:1–25

Duarte P, Fernández-Reiriz MJ, Filgueira R, Labarta U (2010) Modelling mussel growth in ecosystems with low suspended matter loads. J Sea Res 64:273–286

Ertman SC, Jumars PA (1988) Effects of bivalve siphonal currents on the settlement of inert particles and larvae. J Mar Res 46:797–813

Filgueira R, Labata U, Fernándes-Reiriz, MJ (2008) Effect of condition index on allometric relationships of clearance rate in *Mytilus galloprovincialis* Lamarck, 1819. Rev Biol Mar Ocean 43:391–398

Frank DM, Ward JE, Shumway SE, Holohan BA, Gray C (2008) Application of particle image velocimetry to the study of suspension feeding in marine invertebrates. Mar Freshwat Behav Physiol 41:1–18

Fréchette M, Bourget E (1985) Energy flow between the pelagic and benthic zones: factors controlling particulate organic matter available to an intertidal mussel bed. Can J Fish Aquat Sci 42:1158–1165

Fréchette M, Butman CA, Geyer WG (1989) The importance of boundary-layer flows in supplying phytoplankton to the benthic suspension feeder, *Mytilus edulis* L. Limnol Oceanogr 34:19–36

Geer JF, Strikwerda JC (1980) Vertical slender jets. J Fluid Mech 101:53–63

Green S, Visser AW, Titelman J, Kiørboe T (2003) Escape responses of copepod nauplii in the flow field of the blue mussel, *Mytilus edulis.* Mar Biol 142:727–733

Herman PMJ, Middelburg JJ, Koppel JV, Heip CHR (1999) Ecology of estuarine macrobenthos. Adv Ecol Res 29: 195–240

Hussain F, Husain HS (1989) Elliptic jets. Part 1. Characteristics of unexcited and excited jets. J Fluid Mech 208: 257–320

Jones HD, Richards OG, Southern TA (1992) Gill dimensions, water pumping and body size in the mussel *Mytilus edulis* L. J Exp Mar Biol Ecol 155:213–237

Jonsson PR, Petersen JK, Karlsson Ö, Loo LO, Nilsson S (2005) Particle depletion above experimental bivalve beds: *In situ* measurements and numerical modeling of bivalve filtration in the boundary layer. Limnol Oceanogr 50:1989–1998

Jørgensen CB (1990) Bivalve filter feeding: hydrodynamics, bioenergetics, physiology and ecology. Olsen & Olsen, Fredensborg, Denmark, p 140

Jørgensen CB, Famme P, Kristensen HS, Larsen PS, Møhlenberg F, Riisgård HU (1986) The bivalve pump. Mar Ecol Prog Ser 34:69–77

Jørgensen CB, Larsen PS, Møhlenberg M, Riisgård HU (1988) The bivalve pump: properties and modelling. Mar Ecol Prog Ser 45:205–216

Kiørboe T, Møhlenberg F (1981) Particle selection in suspension-feeding bivalves. Mar Ecol Prog Ser 5:291–296

Kwon SJ, Seo IW (2005) Reynolds number effects on the behavior of a non-buoyant round jet. Exp Fluids 38:801–812

Larsen PS, Riisgård HU (1997) Biomixing generated by benthic filter-feeders: a diffusion model for near-bottom phytoplankton depletion. J Sea Res 37:81–90

Lassen J, Kortegård M, Riisgård HU, Friedrichs M, Graf G, Larsen PS (2006) Down-mixing of phytoplankton above filter-feeding mussels — interplay between water flow and biomixing. Mar Ecol Prog Ser 314:77–88

Maar M, Nielsen TG, Petersen JK (2008) Depletion of plankton in a raft culture of *Mytilus galloprovincialis* in Ría de Vigo, NW Spain. II. Zooplankton. Aquat Biol 4:127–141

MacDonald BA, Robinson SM, Barrington K (2009) Evaluating the use of exhalant siphon area in estimating feeding activity of blue mussels, *Mytilus edulis.* J Shellfish Res 28:289–297

Maire O, Amouroux JM, Duchêne JC, Grémare A (2007) Relationship between filtration activity and food availability in the Mediterranean mussel *Mytilus galloprovincialis.* Mar Biol 152:1293–1307

Mann KH, Lazier JRN (1996) Dynamics of marine ecosystems. Biological–physical interactions in the ocean. Blackwell Scientific Publications, Cambridge, MA

Møhlenberg F, Riisgård HU (1978) Efficiency of particle retention in 13 species of suspension-feeding bivalves. Ophelia 17:239–246

Møhlenberg F, Riisgård HU (1979) Filtration rate, using a new indirect technique, in thirteen species of suspension-feeding bivalves. Mar Biol 54:143–148

Newell CR, Campbell DE, Gallagher SM (1998) Development of the mussel aquaculture lease site model MUSMOD: a field program to calibrate model formulations. J Exp Mar Biol Ecol 219:143–169

Newell CR, Wildish DJ, MacDonald BA (2001) The effects of velocity and seston concentration on the exhalant siphon area, valve gape and filtration rate of the mussel *Mytilus edulis.* J Exp Mar Biol Ecol 262:91–111

O'Riordan CA, Monismith SG, Koseff JR (1993) A study of concentration boundary-layer formation over a bed of model bivalves. Limnol Oceanogr 38:1712–1729

Petersen JK, Nielsen TG, van Duren L, Maar M (2008) Depletion of plankton in a raft culture of *Mytilus galloprovincialis* in Ría de Vigo, NW Spain. I. Phytoplankton. Aquat Biol 4:113–125

Plew DR, Enright MP, Nokes RI, Dumas JK (2009) Effect of mussel bio-pumping on the drag on and flow around a mussel crop rope. Aquacult Eng 40:55–61

Price RE, Schiebe FR (1978) Measurements of velocity from excurrent siphons of freshwater clams. Nautilus 92:67–69

Raffel M, Willert CE, Wereley ST, Kompenhans J (2007) Particle image velocimetry–a practical guide. Springer, New York, NY

Riisgård HU (2001a) On measurement of filtration rate in bivalves — the stony road to reliable data, review and interpretation. Mar Ecol Prog Ser 211:275–291

Riisgård HU (2001b) Physiological regulation *versus* autonomous filtration in filter-feeding bivalves: starting points for progress. Ophelia 54:193–209

Riisgård HU, Larsen PS (1995) Filter-feeding in marine macroinvertebrates: pump characteristics, modelling and energy cost. Biol Rev Camb Philos Soc 70:67–106

Riisgård HU, Larsen PS (2005) Water flow analysis and particle capture in ciliary filter-feeding scallops (Pectinidae). Mar Ecol Prog Ser 303:177–193

Riisgård HU, Larsen PS (2010) Particle-capture mechanisms in marine suspension-feeding invertebrates. Mar Ecol Prog Ser 418:255–293

Riisgård HU, Randløv A (1981) Energy budgets, growth and filtration rates in *Mytilus edulis* at different algal concentration. Mar Biol 61:227–234

Riisgård HU, Kittner C, Seerup DF (2003) Regulation of opening state and filtration rate in filter-feeding bivalves (*Cardium edule, Mytilus edulis, Mya arenaria*) in response to low algal concentration. J Exp Mar Biol Ecol 284:105–127

Riisgård HU, Seerup DF, Hjort MH, Glob E, Larsen PS (2004) Grazing impact of filter-feeding zoobenthos in a Danish fjord. J Exp Mar Biol Ecol 307:261–271

Riisgård HU, Lassen J, Kittner C (2006) Valve-gape response times in mussels (*Mytilus edulis*)—effects of laboratory preceding-feeding conditions and *in situ* tidally induced variation in phytoplankton biomass. J Shellfish Res 25: 901–913

Riisgård HU, Lassen J, Kortegaard M, Møller LF, Friedrichs M, Jensen MH, Larsen PS (2007) Filter-feeding zoobenthos and importance of hydrodynamics in the shallow Odense Fjord (Denmark)—Earlier and recent studies, perspectives and modelling. Estuar Coast Shelf Sci 75: 281–295

Schlichting H (1979) Boundary-layer theory. McGraw-Hill, New York, NY

Stamhuis EJ (2006) Basics and principles of particle image velocimetry (PIV) for mapping biogenic and biologically relevant flows. Aquat Ecol 40:463–479

Troost K, Stamhuis EJ, Duren LA (2009) Feeding current characteristics of three morphologically different bivalve suspension feeders, *Crassostrea gigas, Mytilus edulis* and *Cerastoderma edule*, in relation to food competition. Mar Biol 156:355–372

Tweddle JF, Simpson JH, Janzen CD (2005) Physical controls of food supply to benthic filter feeders in the Menai Strait, UK. Mar Ecol Prog Ser 289:79–88

Wildish D, Kristmanson D (1984) Importance to mussel of the benthic boundary layer. Can J Fish Aquat Sci 41: 1618–1625

Wildish D, Kristmanson D (1997) Benthic suspension feeders and flow. Cambridge University Press, Cambridge

Wiles PJ, van Duren LA, Häse C, Larsen J, Simpson JH (2006) Stratification and mixing in the Limfjorden in relation to mussel culture. J Mar Syst 60:129–143

Editorial responsibility: Roger Hughes, Bangor, UK

Submitted: December 23, 2010; Accepted: June 21, 2011
Proofs received from author(s): August 25, 2011